RSC Advances

ROYAL SOCIETY OF CHEMISTRY

www.rsc.org/advances

Preparation and properties of magnetic Fe_3O_4/poly(pyrimidine-amide) nanocomposites: selective polyamidation of a bis(amino-pyrimidine-diol) compound in an ionic liquid

Mehdi Taghavi, Raouf Alizadeh, Mousa Ghaemy*

Polymer Chemistry Research Laboratory, Faculty of Chemistry, University of Mazandaran, Babolsar, 47416-95447, Iran.

This work reports preparation of magnetic nanocomposites (MNCPPA)s from interfacial reaction between multifunctional poly(pyrimidine-amide)s (PPAs) and epoxide functionalized magnetic Fe_3O_4 nanoparticles. In this regard, organosoluble PPAs were synthesized selectively from polycondensation of bis(2-aminopyrimidine-4,6-diol) compound (DATPhP) with different aromatic and aliphatic dicarboxylic acids in a mixture of ionic liquid(IL)/triphenyl phosphate (TPP) at 110 °C for 2.5 h. The PPAs have weight-average molar mass (M_w) up to 49500 g mol^{-1}, glass transition temperatures (T_g) up to 240 °C and 10% weight loss temperatures ($T_{10\%}$) up to 486 °C (in N_2). The results showed that strong chemical bonding between modified Fe_3O_4 nanoparticles and PPAs chains reduced solubility and enhanced thermal and mechanical properties of the composites. Also, antibacterial and antioxidant activities of the monomer, PPAs and MNCPPA were studied.

Keywords: Nanocomposite, Poly(pyrimidine-amide), Ionic liquid, Selective polyamidation, Surface modification, Properties

* Corresponding author. Tel.: +98-112-5342353; FAX: +98-112-5342350.
E-mail address: ghaemy@umz.ac.ir (Mousa Ghaemy).

Introduction

In recent years much attention has been given to reusability of solvents and catalysts for the development of cost-effective processes.[1] Ionic liquids (ILs) are organic salts that act much like good organic solvents dissolving both polar and nonpolar species,[2-4] they are non-volatile and easily recyclable reaction media of high thermal and chemical stabilities. Most polycondensation studies were relative to the synthesis of aromatic polymers such as polyamides, polyimides, polyhydrazides or polyoxadiazoles in a range of conventional ionic liquids.[5-9] However, the synthesis of polyesters in ionic liquids has been confronted with some challenges. A few studies were undertaken on the synthesis of polyesters in ionic liquids, mainly in Brønsted acid ionic liquids (BAILs) [10-12] and in dialkylimidazolium bis(trifluoromethylsulfonyl) amide salts by post-polycondensation of oligoesters which required high temperature (160 ºC), reduced pressure (50 Pa), long reaction time (24 h) with addition of a metal (Sn^{2+}) catalyst, and enzymatic methods yielded low molar mass polyesters.[13,14] Pyrimidine and purine compounds play an essential role in several biological processes and have very important chemical and pharmacological properties. The pyrimidine nucleus is embedded in a large number of alkaloids, drugs, antibiotics, agrochemicals, and antimicrobial agents.[15,16] The simultaneous presence of an azide group and an o-phenol moiety in a pyrimidine molecule is certainly of scientific and practical interest, since the formation of a strong intramolecular hydrogen bond between the phenolic hydroxyl and the aza atom of the heteroaromatic ring has an effect on the reactivity.[17] The unique magnetic properties of Fe_3O_4 nanoparticles and its composites have led to their implementation in many technological as well as biomedical applications in a wide variety of fields such as data

storage, catalysis, gas sensors, magnetic resonance imaging, wastewater remediation, bioseparation, medicine etc.[18-20] The magnetic nanoparticles tend to form agglomerates by interaction among themselves or with biological molecules and precipitate out of the system.[21-23] Various protection strategies have been developed for the chemical stabilization of the nanoparticles,[24-26] among which the surface coating not only protects the nanoparticles from agglomeration and ensures their better dispersibility but also renders functionalisation to the system.

In this work, following our previous work,[6] we are reporting selective polyamidation for a new interesting and multifunctional bis(2-aminopyrimidine-4,6-diol) compound, DATPhP, with different dicarboxylic acids in the mixture of IL/TPP. DATPhP has antibacterial and antioxidant activity and is fluorescent due to bearing carbazole ring. The prepared functionalized poly(pyrimidine-amide)s (PPAs) were characterized by FT-IR, ^{1}H NMR and GPC and used for preparation of magnetic nanocomposites (MNCPPA)s that polymer chains are chemically bound with epoxide functionalized Fe_3O_4 nanoparticles. The MNCPPAs were characterized by FT-IR, XRD, VSM and AFM techniques and their properties such as solubility, thermal, photophysical and mechanical were measured and compared with those of PPAs. Also, monomer, PPAs and a composite were tested for antimicrobial and antioxidant activities.

Results and discussion

Synthesis and characterization of DATPhP (1)

This manuscript reports selective polyamidation of a new compound, DATPhP, with several commercial aliphatic and aromatic diacids in an imiazolium-based IL. For this purpose, as illustrated in **Scheme 1**, compound 1 (DATPhP) was successfully synthesized

by nucleophilic reaction between 2-amino-4,6-dihydroxypyrimidine and 9-ethyl-3-carbazolecarboxaldehyde, see ESI (section S1). The structure of DATPhP was identified by elemental analysis, and FT-IR and ^{1}H NMR spectroscopy. FT-IR spectrum in **Fig. 1** shows absorption band of the amine group at 3400 cm^{-1} as doublet, ^{1}H NMR spectrum in **ESI (Fig. 1S)** shows protons of aliphatic -C-H, amine and hydroxyl groups at 5.53, 6.78 and 10.40-1053 ppm, respectively. ^{13}C NMR spectrum of compound DATPhP showed 23 different carbons for the aromatic and heterocyclic rings.

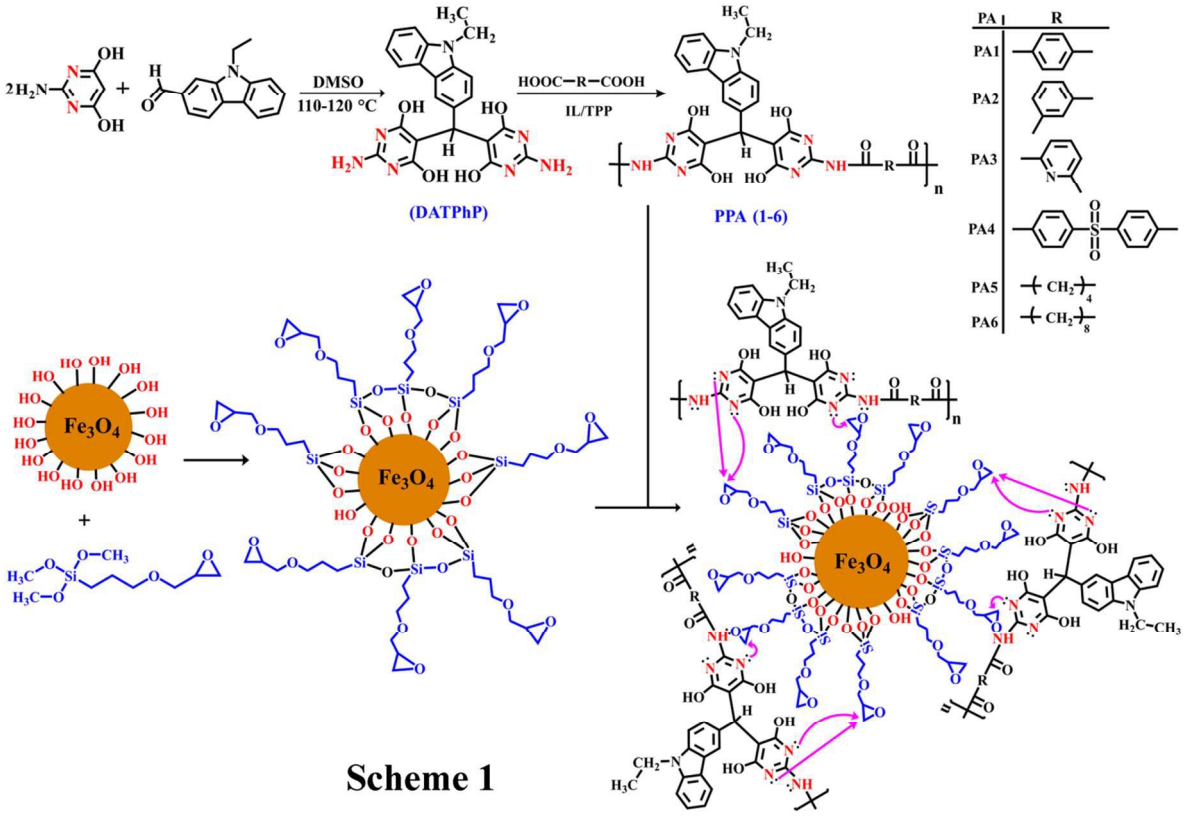

Scheme 1

Scheme 1 Illustration of synthesis of target compound (DATPhP), PPAs and nanocomposite.

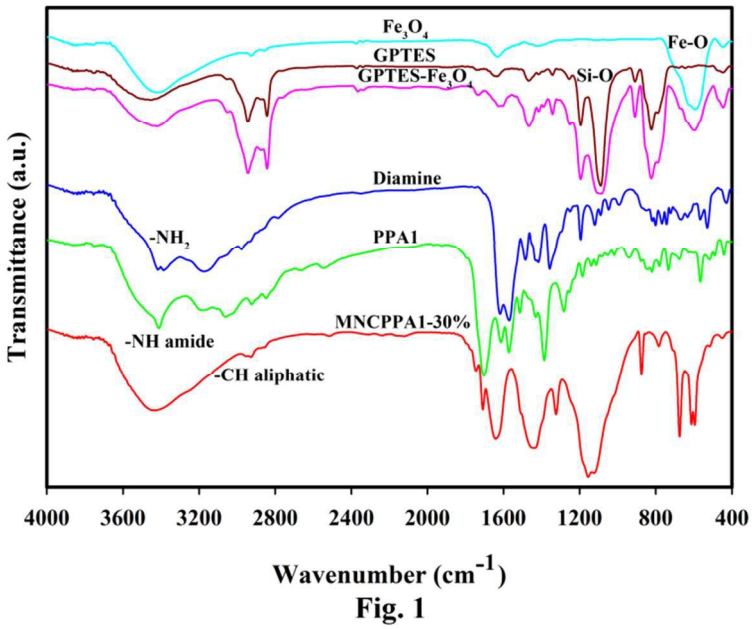

Fig. 1

Fig. 1 FT-IR spectra of Fe_3O_4, GPTES, GPTES-Fe_3O_4, DATPhP, PPA1 and MNCPPA1-30%.

Synthesis and characterization of PPAs and nanocomposites

In this work, a simple and efficient method was used for the selective polyamidation of DATPhP with several commercial diacids in the mixture of IL/TPP without using NMP/Py/LiCl mixture which is required in the conventional direct polycondensation by Yamazaki.[27] The ILs based on 1,3-dialkylimidazolium cations have gained considerable interest as promising alternative green solvents in polymer synthesis.[3-6] Therefore, ionic liquid $[1,3\text{-Propyl2im}]^{+}Br^{-}$ was selected as the reaction medium for polycondensation of DATPhP with different dicarboxylic acids.[6] The PPAs synthesis is reported in ESI (Section S2) and polymers designation are shown in **Scheme 1**. The PPAs obtained in IL/TPP mixture were brown powder with good yields of 80-95% after removal of low molecular weight fractions by using hot methanol extraction, and they were all soluble in aprotic organic solvents. This demonstrates the beneficial effect of IL for the synthesis of

thermoplastic PPAs from bis(2-aminopyrimidine-4,6-diol) compound, in addition to other useful factors such as the non-volatility of IL, low reaction time (2.5 h), no environmental pollution, and no need to remove chemicals such as NMP, LiCl and Py. The reason for the selectivity can be due to reaction of phenolic hydroxyl groups of DATPhP with the ionic liquid and formation of phenolic salt, while the amine groups remain free to react with the carboxylic acid groups to give amide linkages. Inherent viscosities of these PPAs in NMP (0.5 g/dL) were in the range of 0.49 - 0.74 dL/g. The elemental analysis results were in good agreement with the calculated percentages for carbon, hydrogen and nitrogen contents in PPAs repeating units. The weight average molecular weights (M_w) of PPAs, as listed in **Table 2**, were in the range of 28400-49500 g/mol with MMD of 1.41-1.97. The relatively high molecular weights of these polymers can be due to the fact that IL can dilute highly viscous polymer solution and facilitate the elimination of the byproduct, thus shifting the equilibrium. FT-IR spectrum of PPA1, in **Fig. 1**, exhibits the characteristic absorption bands of N-H stretching of amide and phenolic hydroxyl groups at 3200-3400 cm^{-1}, C=N stretching at 1290 cm^{-1}, and C=O stretching at 1680 cm^{-1}. The ^1H NMR spectra of PPA5 and PPA4 in **ESI (Fig. 2S)**, shows the N-H proton of amide groups at 11.06-11.08 ppm and phenolic hydroxyl groups at 11.87 ppm. The signals of aromatic and aliphatic protons appeared in the range of 7.11-8.07 ppm and 1.31-5.02 ppm, respectively. In order to improve dispersion of nanoparticles in polymer matrix and enhance the interfacial interaction between the two phases, GPTES molecules were linked to the Fe_3O_4 surface via Fe-O-Si bonds. This was achieved by condensation of hydroxyl groups (-OH) on the surface of activated Fe_3O_4 with the hydrolysable methoxy groups ($-OCH_3$) of GPTES. Synthesis of Fe_3O_4 nanoparticles and their surface

modification with GPTES is reported in ESI (Section S3 and S4). FT-IR spectrum of Fe_3O_4 in **Fig. 1** presents absorption bands at 586 cm^{-1} related to Fe-O vibration mode, at 890 cm^{-1} and 790 cm^{-1} due to stretching of Fe–O–H and at 3400 cm^{-1} to the characteristic stretching vibration of hydroxyl group (-OH). FT-IR spectrum of GPTES-Fe_3O_4 in **Fig. 1** presents stretching vibrations of Si-O link and epoxide group at 900-1100 cm^{-1}, stretching vibration of hydroxyl group on the surface of Fe_3O_4 at 3400 cm^{-1}, and bending and stretching vibrations of C-H of methylene linkage at 1380 and 2906-2857 cm^{-1}, respectively. The above interpretations are enough to suggest that GPTES is bound on the surface of Fe_3O_4 particles. Magnetic GPTES-Fe_3O_4/PPA nanocomposite (MNCPPA) was prepared by solution blending (at 80 °C) via interfacial reaction between surface epoxide groups on GPTES-Fe_3O_4 and tertiary amines of PPA chains, as illustrated in **Scheme 1**. FT-IR spectrum of nanocomposite containing 20 wt% GPTES-Fe_3O_4 exhibits changes in the absorption bands at 1600 cm^{-1} and 3400 cm^{-1} in comparison with the spectrum of PPA1, **Fig. 1**. These changes can be due to protonation of tertiary amines with the epoxide group of GPTES-Fe_3O_4. Previous studies on the adduct formation between 1-substituted imidazole [28-30] and triazole [30] with the epoxide group suggested that reaction between more basic pyridine-type nitrogen with the epoxide group leads to a zwitter ionic structure, as shown in Scheme 1. DSC technique was also used to prove the occurrence of chemical reaction between epoxide groups of GPTES-Fe_3O_4 and tertiary amines of PPA chain when composite is prepared by solution blending at 70 °C. In this regard, mixture of PPA5 and GPTES-Fe_3O_4 was heated in the DSC sample pan and an exothermic peak appeared in the temperature range of 80-100 °C, as can be seen in **Fig. 2A**. While composite, MNCPPA5-10%, prepared by solution

blending at 70 °C did not show exothermic peak in the region of 80-100 °C, as can be observed in **Fig. 2A**. The absence of exothermic peak indicates that epoxide groups in GPTES-Fe_3O_4 nanoparticles reacted with the tertiary amines in PPA chains during solution blending at 70 °C. The above interpretations, and also the insolubility of nanocomposites in organic solvents, are enough evidences to suggest that GPTES-Fe_3O_4 is chemically linked with the PPA chains. **Fig. 2B** shows the TGA curves of Fe_3O_4 and GPTES-Fe_3O_4. It can be seen that the weight loss is 7% in temperature range of 0-200 °C for Fe_3O_4 (almost no weight loss over 300 °C), it is mainly due to the loss of absorbed moisture. The weight of GPTES-Fe_3O_4 decreases quickly over 200 °C and the loss is about 20% over 400 °C, which can be attributed to the thermal decomposition of GPTES at high temperature. By comparison of the TGA curves in **Fig. 2B**, it can be deduced that the maximum mass fraction of GPTES on the surface of Fe_3O_4 is about 20%. XRD patterns for PPA5, GPTES-Fe_3O_4, and MNCPPA5-20% are shown in **ESI** (**Fig. 3S)**. According to the XRD patterns, neat PPA5 is totally amorphous in nature which does not show any sharp diffraction peaks, but the composite containing 20 wt% GPTES-Fe_3O_4 expressing that the crystal structure of Fe_3O_4 was not altered due to the presence of PPA5. The peaks intensity depends on the amount of modified GPTES-Fe_3O_4 in the composite.

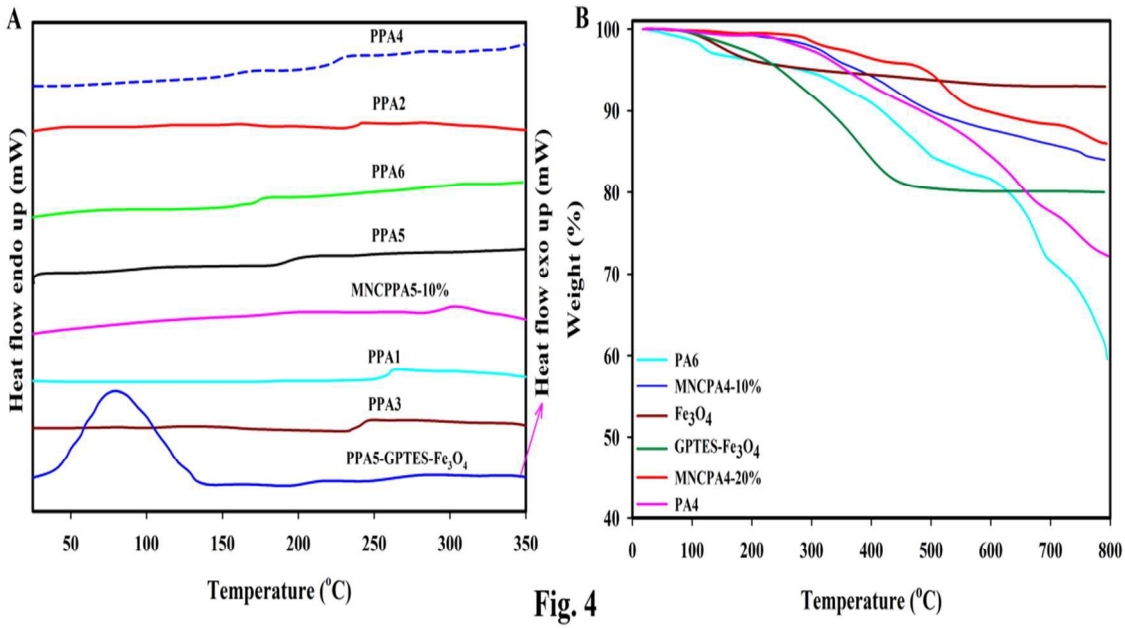

Fig. 4

Fig. 2 (A) DSC curves of PPAs, MNCPPA5-10% and GPTES-Fe_3O_4/PPA mixture, (B) TGA curves of Fe_3O_4, GPTES-Fe_3O_4, PPAs, MNCPPA4-10% and MNCPPA4-20% under N_2 at 10 ^oC/min.

Properties of PPAs and nanocomposites

Solubility and moisture absorption

The solubility behavior of PPAs and nanocomposites was tested qualitatively in various organic solvents. All PPAs exhibited excellent solubility in polar aprotic solvents such as NMP, DMAc, DMF, DMSO and even in less polar solvents like pyridine and THF. The good solubility should be due to presence of different functional groups in the polymer backbone such as phenol hydroxyl groups, bulky heterocyclic pendant, and aliphatic linkage. These factors and also the amorphous nature contributed to the enhanced solubility of these PPAs through better penetration of solvent molecules, formation of H-bonding and dipole-dipole interaction with polar molecules of organic solvents. However, aliphatic PPAs such as PPA5 and PPA6 exhibited better solubility behavior in less polar solvents such as THF and m-cresol than aromatic PPAs. The presence of methylene units

instead of rigid phenyl improved the solubility of PPA5 and PPA6. Composites of PPA with 5 wt% modified Fe_3O_4 (mNP) showed partial solubility in highly polar solvents by heating at 60 ºC. This indicates that 5 wt% mNP is not enough to form a complete network with PPA, thus some of low molecular weight fractions dissolved by heating. However, nanocomposites containing more than 10 wt% mNP did not dissolve indicating formation of chemical bonds between mNP and PPA chains. The water uptake determines the final application of high performance materials. The absorbed water diminish T_g and influence mechanical and electrical properties, but in membrane technology, greater water uptake implied better performance. Because of the presence of bulky pendant in the PPA chain which increases the free volume, functional groups such as amide and hydroxyl can easily and effectively interact with water molecules. The results obtained from moisture absorption by PPAs, as listed in **Table 1**, showed that moisture intake varied from 8.39% to 16.45%. The highest moisture absorption for PPA4 and PPA3 can be due to presence of SO_2 linkage in PPA4 and nitrogen atom in PPA3 which form hydrogen bonding with water molecules. The least water absorption of PPA5 and PPA6 can be due to presence of hydrophobic methylene groups.

Table 1 Average molecular weights, viscosity and solubility of PPAs and nanocomposites

Code	η_{inh} (dL/g)[a]	M_n (g/mol)	M_w (g/mol)	Moisture Absorption (%)	DMSO	DMAc	DMF	NMP	Py	THF	*m*-cresol
PPA1	0.66	29100	41000	12.11	++	++	++	++	+	±	±
PPA2	0.58	16350	32200	10.97	++	++	++	++	+	±	±
PPA3	0.69	27650	44520	13.02	++	++	++	++	+	±	±
PPA4	0.74	31100	49500	16.45	++	++	++	++	+	±	±
PPA5	0.54	18400	31850	9.74	++	++	++	++	++	+	+
PPA6	0.49	15600	28400	8.39	++	++	++	++	++	+	+
MNCPPA1-5%	-	-	-	-	±	±	±	±	-	-	-
MNCPPA1-10%	-	-	-	-	-	-	-	-	-	-	-
MNCPPA5-5%	-	-	-	-	±	±	±	±	-	-	-
MNCPPA5-10%	-	-	-	-	-	-	-	-	-	-	-
MPPA1'	-	-	-	-	-	-	-	-	-	-	-

Morphology and disperse ability of GPTES-Fe_3O_4

In order to examine the microstructures and nanofiller distribution within the nanocomposites, SEM and AFM analysis were conducted. Typical surface SEM images of three different samples of neat Fe_3O_4 nanoparticles, GPTES-Fe_3O_4, MNCPPA4-20% and TEM image of MNCPPA6-20% are illustrated in **Fig. 3**. As can be seen in these images, the appearance and size of the particles changed as the surface of the bare Fe_3O_4 (image **A**) was covered by ~20% GPTES (image **B**) and by 80% PPA4 (image **C**). As can be clearly seen in image C, the surface of Fe_3O_4 particles is fully covered by the organic phase. This can also demonstrate a good adhesion and, as suggested before, strong interfacial bonding between polymer chains and GPTES-Fe_3O_4 particles. TEM micrograph of the hybrid film in **Fig. 3(D)** shows dispersion of GPTES-Fe_3O_4 particles in the polymer matrix and reveals the core-shell structure. The surface morphology of GPTES-Fe_3O_4 and MNCPPA4-20% was also examined by AFM measurements, shown in **ESI** (**Fig. 4S)**. It can be seen in these figures that the surface roughness is rather small for the case of GPTES-Fe_3O_4 with an average size of 70 nm, while the surface of MNCPPA4-20% sample showed many hills and valleys with average size of 27 nm. These changes in morphology and size of particles show that there is a good dispersion of GPTES-Fe_3O_4 nanoparticles in the polymer matrix, where sharp points are referred to Fe_3O_4 nanoparticles.

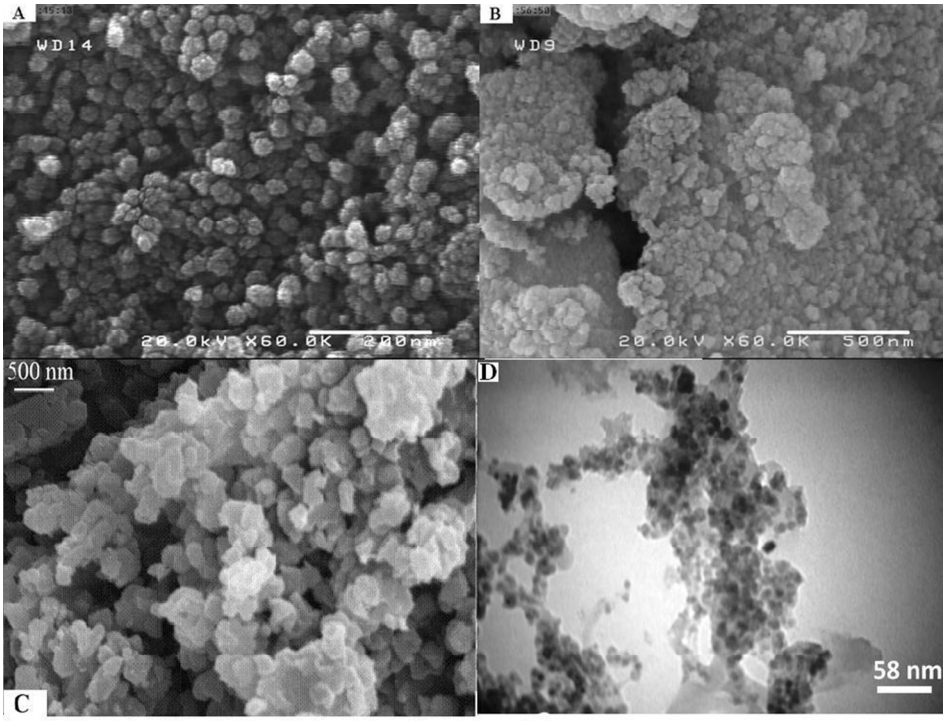

Fig. 3 FESEM image of Fe_3O_4 (A), GPTES-Fe_3O_4 (B), MNCPPA4-20% (C) and TEM image of MNCPPA4-20% (D).

Photophysical properties

The photophysical properties of PPAs and nanocomposites were investigated by using UV-vis and fluorescence spectroscopy. The absorption and fluorescence spectra of PAs and nanocomposites films are shown in **Fig. 4**. The absorption spectra of PPAs in dilute NMP solution (0.2 g/dL) and in films, **Fig. 4A**, were nearly identical and the maximum absorption wavelengths (λ_{ab}) were at λ_{ab}= 277nm (carbazole ring, which shows a relatively small energy band gap for $\pi \rightarrow \pi^*$ transition) and at λ_{ab} = 442 nm, as listed in **Table 2**. Reasonably, this could be attributed to the all aromatic structure possessing substituted imidazole pendant attached to the aromatic backbone. To investigate the

fluorescence emission of PPAs, an excitation wavelength of 285 nm was used in all cases. The fluorescence emission spectra of PPAs are shown in **Fig. 4B**.

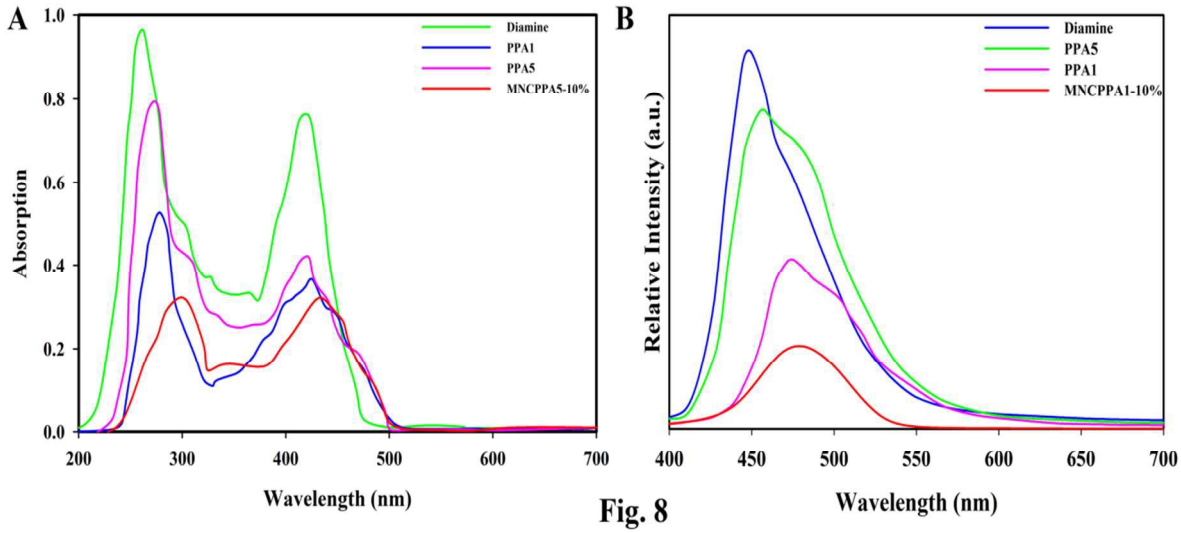

Fig. 4 UV-vis and fluorescence spectra of PPAs and nanocomposites.

To measure the photoluminescence (PL) quantum yields (Φ_f), dilute PAs solutions (0.2 g/dL) in NMP were prepared. A 0.10 N solution of quinine in H_2SO_4 (Φ_f= 0.53) was used as a reference.[31] The solution and thin films of PPAs showed broad fluorescent emission spectra with the maximum wavelengths in the range of λ_{em} = 460-486 nm and Φ_f = 16-34 %, as listed in **Table 2**. The aliphatic PPA5 and PPA6 exhibited blue emission (λ_{em}= 460-471 nm) with the highest Φ_f values of 31 and 34%, respectively. The aromatic PPAs exhibited green emission (λ_{em} = 477-486 nm) and Φ_f in the range of 13–19 %. The blue shift and higher intensity of PL of aliphatic PPAs compared with the PL of aromatic PPAs could be attributed to the effectively reduced conjugation and capability of charge transfer complex formation by aliphatic diacids in comparison with the electron-donating amino unit and the strongly electron-accepting aromatic diacid unit.[30] The absorption and emission spectra of the representative nanocomposite films are shown in **Fig. 4** (**A** and

B). **Table 2** lists some important photophysical data obtained from films and suspension solution of composites containing 10 wt% mNP. The nanocomposites also showed absorption at λ_{ab} = 281nm and at 457 nm, emission in the range of λ_{em} = 462-490 nm. As can be seen in **Fig. 4B** and in **Table 2**, similar to aliphatic PPAs their nanocomposites (NCPA5-10% and NCPA6-10%) also showed blue shift, in comparison with the nanocomposites of aromatic PPAs which showed green shift.

Table 2 Optical properties data of PPAs and nanocomposite.

Code	λ_{ab}(nm)[a]	λ_{em}(nm)[a]	λ_{ab}(nm)[b]	λ_{em}(nm)[b]	Φ_f[a] (%)
PPA1	278,425	473	286,438	477	19
PPA2	276,422	471	279,433	473	17
PPA3	276,424	476	282,440	479	16
PPA4	289,442	481	295,449	486	13
PPA5	274,421	463	277,431	471	31
PPA6	273,421	456	277,431	460	34
MNCPPA1-10%	-	-	288,441	482	-
MNCPPA2-10%	-	-	283,435	475	-
MNCPPA3-10%	-	-	287,443	486	-
MNCPPA4-10%	-	-	296,457	490	-
MNCPPA5-10%	-	-	281,433	475	-
MNCPPA6-10%	-	-	281,433	462	-

Polymer concentration of 0.20 g/dL in NMP.
[a,b]UV-visible absorption and fluorescence emission spectra of the PPAs and nanocomposites (10% mNP) in solution (a) and in films (b), respectively.
[c]Fluorescence quantum yield relative to 10^{-5} M quinine sulfate in 1 N H_2SO_4 (aq) (Φ_f = 0.55) as a standard.

Antioxidant activity

Antioxidant activity was measured using the DPPH assay according to the reported method with slight modification.[32] DPPH evaluation is standard assay in antioxidant activity studies and offers a rapid technique for screening of specific compounds. The DPPH free radical with an odd electron gives a maximum absorption at 517 nm (purple color). When the composites react with DPPH, the free radical becomes paired off in the presence of a hydrogen donor and reduces to the DPPHH or converts to DPPH anion

through electron transfer reaction (in **ESI**, **Scheme 1S)**. Consequently, the absorbance decreases for the DPPH. The antioxidant activities of DATPhP, PPAs, and MNCPPA4-5% are shown in **Fig. 5**. The radical scavenging activity is expressed in percentage by the given relation:

$$\% \text{ DDPH inhibition} = \frac{A_c - A_s}{A_s} \times 100$$

where A_b is the absorption of the blank (DPPH + EtOH) and A_s is the absorption of the sample (DPPH + Sample + EtOH). As can be seen in **Fig. 5**, PPA4 shows higher antioxidant activity than PPA1 which can be due to presence of sulfoxide (-SO_2-) in PPA4 chain. The nanocomposite MNCPPA4 containing 5 wt% of GPTES-Fe_3O_4 showed much higher antioxidant activity than neat PPA1 and PPA4 polymers.

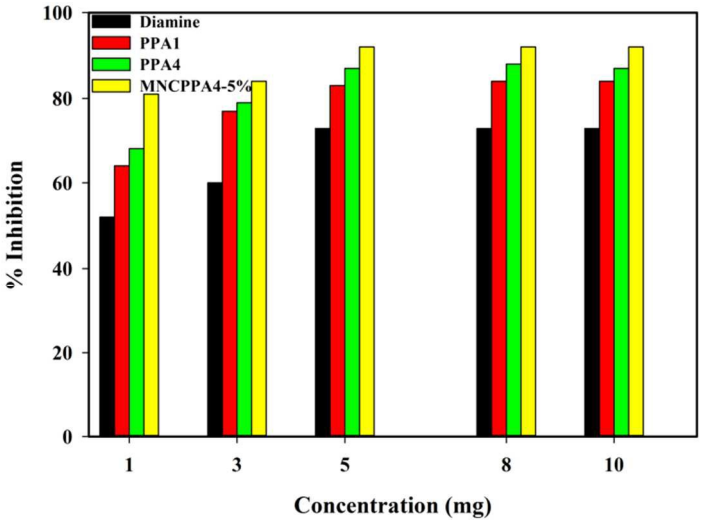

Fig. 5 Antioxidant activity of DATPhP, PPA1, PPA4 and MNCPPA4-5%.

Antimicrobial activities

The antimicrobial activities of the synthesized compounds were evaluated against P. aeruginosa, S. aureus (Gram negative bacteria), K. pneumoniae (gram negative bacteria), A. oryzae, and A. niger (fungi). An agar-well diffusion test was performed in each case. The zone of inhibition (in mm) around the well was determined and results are listed in **Table 3**. Gentamycin and fluconazole were used as the reference standards for antibacterial and antifungal activity, respectively.[33] In case of antibacterial activities, PPA4 and nanocomposite MNCPPA4-5% showed maximum zone of inhibition against *S. aureus* and *P. aeruginosa*. Also, the nanocomposite MNCPPA4-5% showed maximum activity against growth of *A. oryzae* and *A. niger* fungi. From the results of antimicrobial and antifungal activities, it is revealed that composite of PPA polymers containing Fe_3O_4 nanoparticles showed maximum inhibition activities.

Table 3 Antimicrobial activity results of compounds.

Code	Antibacterial activity (zone of inhibition in mm)		Antifungal activity (zone of inhibition in mm)	
	S. aureus	*P. aeruginosa*	*A. oryzae*	*A. niger*
Diamine	7	8	6	7
PPA1	10	10	9	11
PPA4	12	13	11	11
MNCPPA4-5%	12	14	13	13
Gentamycin	15	16	-	-
Fluconazole	-	-	16	16

Mechanical properties

The tensile stress-strain curve is a tool to provide data on toughness (area under the curve), ultimate tensile strength, ultimate elongation at break and Young's modulus. The data obtained from typical stress-strain curves for PPAs and nanocomposites are

summarized in **Table 4**. An average of five individual measurements was used for each sample. The PPAs showed tensile strength in the range of 86-114 MPa, elongation to break of 12-19%, and initial modulus of 1.52-1.98 GPa. PPA1" which was prepared in the mixture of TPP/Py/NMP/LiCl, as can be seen in the **Table 4**, is a brittle polymer with low elongation (1.43%) and high Young's modulus (3.84 GPa). The area under the stress-strain curve is used to measure the fracture energy or static toughness of the polymer and depends on the molecular weight and intermolecular interactions. PPA4 showed the highest tensile strength and toughness due to higher molecular weight and more symmetrical structure sulfone unit in comparison with the other PPAs. PPA5 and PPA6 showed the lowest strength and elongation due to presence of aliphatic chain in the backbone and lower molecular weights in comparison with the other PPAs. From the table, we can see the noticeable trend of tensile strength of specimens increased when increasing the mNP amount. The tensile strength of PPA4 increased from 128 MPa to 141 PMa for MNCPPA4-20%, and simultaneously, the tensile elongation decreased from 19% to 11%. The enhancement of tensile strength corresponds to the forecast, as mentioned before, that mNP could play a reinforcing role in the composite. It might be ascribed to the presence of chemical interactions between mNP and hydroxyl groups in the PPAs chains and formation of cross-links. As we know, elongation at break is a crucial parameter to judge the plasticity or ductility of the polymer. Generally, the addition of inorganic particles into polymers, and in this case formation of cross-links, lowers the elongation at break.

Table 4 Mechanical and thermal properties of PPAs and nanocomposites.

Code	Tensile[a]	Modul.	Elon.%	T_g (°C)[b]	T_{10} (°C)[c]	C. Y.[d]	LOI (%)[e]
PPA1	114.01	1.73	16.08	257	454	70	45
PPA1'	134.49	3.84	1.43	-	468	74	47
PPA2	112.35	1.71	15.17	238	442	66	44
PPA3	122.68	1.88	17.44	240	467	70	45
PPA4	128.10	1.98	18.91	222	486	72	46
PPA5	96.85	1.59	13.10	195	429	63	43
PPA6	85.73	1.52	12.39	174	420	59	41
NCPPA1-10%	119	1.99	13.03	304	479	74	47
NCPPA2-10%	124	1.91	12.72	-	473	73	47
NCPPA3-10%	132	2.08	15.06	-	501	75	47
NCPPA4-5%	130	2.13	17.45	293	498	77	48
NCPPA4-10%	134	2.36	15.78	313	504	84	51
NCPPA4-15%	139	2.41	14.29	-	566	84	51
NCPPA4-20%	141	2.47	11.53	-	581	86	52
NCPPA5-10%	106	1.87	9.40	298	485	68	45
NCPPA6-10%	100	1.80	7.37	264	472	65	43

[a]Film stored in a 80% relative humidity atmosphere before tensile test.
[b]T_g was recorded by DSC at 10 °C/min in N_2.
[c]$T_{10\%}$ was recorded by TGA at 10 °C/min in N_2.
[d]C.Y.= Char yield, weight% of material left at 800 °C in N_2.
[e]Limiting oxygen index percent evaluating at char yield 800 °C.
PPA1': This PPA was prepared in the mixture of TPP/NMP/Py/LiCl.

Thermal properties

The thermal behavior data of these PPAs and nanocomposites were assessed by using DSC, DMTA and TGA analysis. The glass-transition temperature values (T_gs) of PPAs were obtained from DSC curves with a heating rate of 10 ºC min^{-1} under N_2. **Fig. 2A** shows DSC curves of PPAs, neither crystallization exotherms nor melting endotherms were observed in the range of 35-400 ºC, so that these PPAs were considered to be essentially amorphous. The amorphous nature of these PPAs can be attributed to their bulky pendant group which decreased the inter-chain interaction resulting in loose

polymer chain packaging and aggregates. The T_g values were read at the middle of the first break down observed in the DSC curves, and found to be in the range of 174-313 ºC, as listed in **Table 4**. In general, molecular packing and chain rigidity are among the main factors influencing on T_g values. Therefore, the increased rotational barrier caused by the bulky pendant in the monomer 1 and side chain-side chain and side chain-main chain interactions enhanced T_g values. As anticipated, the T_g values of these PPAs also depend on the stiffness of dicarboxylic acid component in the polymer chain and the increasing order of T_g generally correlated with that of chain rigidity. PPA6 and PPA5 obtained from aliphatic dicarboxylic acid, showed lower T_g values (174 ºC and 195 ºC, respectively) because of the presence of flexible aliphatic unit and their low rotation barrier, and the highest T_g value of 257 ºC was observed for PPA1 derived from terephthalic acid. T_g values of composites showed dependence on the amount of mNP particles. As shown in **Table 4**, composites of aromatic PPAs containing more than 10 wt% mNP did not show T_g up to 400 ºC, while T_g of PPA4 increased from 222 ºC to 313 ºC when contains 10 wt% mNP. The thermo-stability of the resulting PPAs and nanocomposites was evaluated by TGA under N_2 atmosphere at a heating rate of 10 ºC min^{-1}. **Fig. 2B** presents TGA curves of the PPAs, and the corresponding 10% weight loss temperatures ($T_{10\%}$) determined from the original curves in N_2 (420-486 ºC) are listed in **Table 4**. Char yield (CR) can be used as criteria for evaluating limiting oxygen index (LOI) of the polymers in accordance with Van Krevelen and Hoftyzer equation,[34] LOI= 17.5 + 0.4CR. In general, when the LOI of a polymer is higher than 26% it is considered to be flammable. For these PPAs, LOI values were calculated based on their char yields at 800 °C. According to **Table 4**, thermal stability of the aromatic PPAs in N_2 appeared

in the 442-486 ºC range in terms of $T_{10\%}$ values, compared to 420-429 ºC for the aliphatic PPAs. This can be pertained to the rigid structure of aromatic diacids compared to the flexible structure of aliphatic diacids. **Fig. 2B** shows TGA curves of nano Fe_3O_4, mNP, MNCPPA4-10% and MNCPPA4-20%, and the thermal data extracted from the original curves are listed in **Table 4**. The $T_{10\%}$ value of MNCPPA4-20% in comparison with the same pure PPA4 has increased from 486 ºC to 581 ºC with the char yield from 72% to 86% in N_2. It is clear that the existence of inorganic material in polymer matrix and its chemical interactions with the polymer shifted decomposition temperature towards higher temperatures indicating enhanced thermal stability of the composite with mNP loading. The viscoelastic behavior of the representative PPAs and nanocomposites was determined by using DMTA. Tan δ curves are shown in **Fig. 6**. Measurement of tan δ values was carried out to relate the viscoelastic behavior and PPAs molecular structure and mNP content in the composites. The increase in the T_g (maximum of tanδ curve) values indicates that a change in the viscoelastic behavior of the nanocomposite films from liquid like to solid-like occurs. As already has been discussed, mNP particles and PPA chains have definitely been involved in reactions of cross-links formation. These immobilize the polymer chains at elevated temperatures. Thermoplastic response of PPAs and their nanocomposites was determined by plotting storage modulus against testing temperature. **Fig. 6** shows the storage modulus values as a function of varying wt% of mNP particles. It was observed that with increasing wt% of mNP particles the value of storage modulus of composite increases.

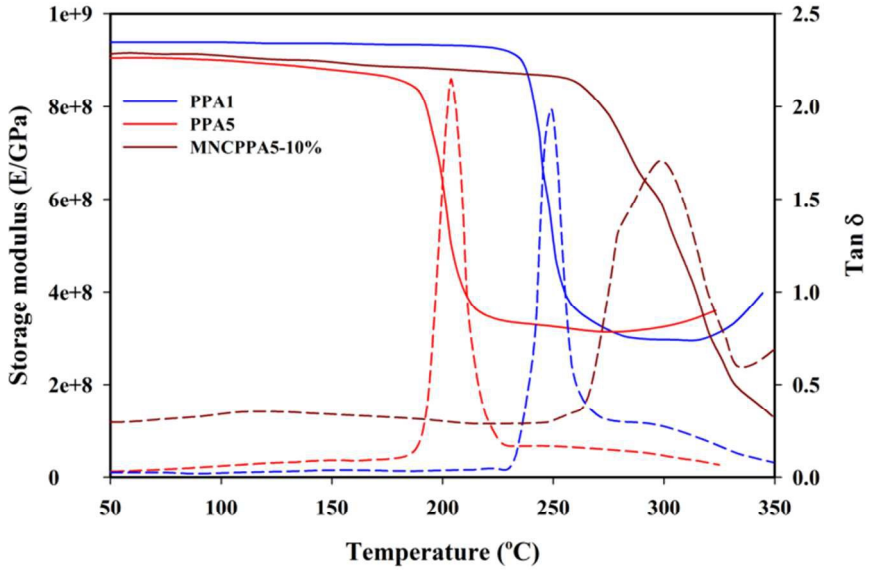

Fig. 10

Fig. 6 DMTA curves of tan δ and storage modulus of PPA1, PPA5 and NCPA5-10%.

Analysis of magnetic properties

Vibrating sample magnetometry (VSM) was employed to study the magnetic properties of the prepared Fe_3O_4, GPTES-Fe_3O_4 and composite. The magnetic hysteresis loops of these materials were determined as a function of applied magnetic field at room temperature and the results are illustrated in **Fig. 7**. It is vitally important that materials which are suggested for the sorbents should possess sufficient magnetic and superparamagnetic properties. As can be seen, naked Fe_3O_4 nanoparticles have high saturation magnetization of 58 emu/g at 8000 Oe, with remanence and coercivity of zero in the absence of external magnetic field. The very weak hysteresis confirms that these materials have superparamagnetic properties at room temperature, which implies that the sample keeps no remanence in the absence of an external magnetic field. The saturation magnetization value for GPTES-Fe_3O_4 and for composite with 20 wt% GPTES-Fe_3O_4 was 19 emu/g and 9 emu/g, respectively. Compared to the naked Fe_3O_4 (58 emu/g),

decrease in the magnetic strength of GPTES-Fe_3O_4 and composite can be due to surface coating of Fe_3O_4 with GPTES and PPA chains. However, the saturation magnetization is sufficiently enough which makes the composite very susceptible to magnetic fields and separation from a suspension can be preceded easily and quickly with a conventional magnet, as shown in **Fig. 7**. The magnetic properties (saturation magnetization and superparamagnetic behavior) of the present polymer-based nanoparticles can also be of interest for drug targeting purposes and also for bioapplications, such as magnetic resonance imaging (MRI) agents, where Ms of 7-22 emu g^{-1} is usually needed.[35]

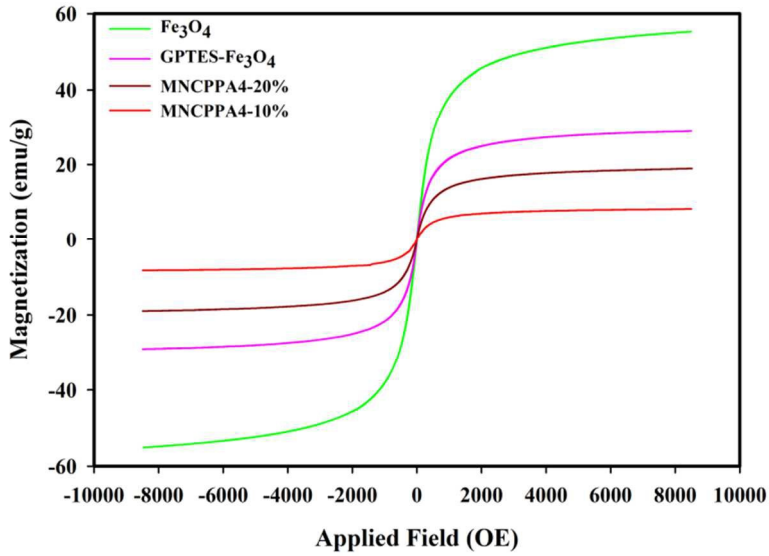

Fig. 11

Fig. 7 VSM images of Fe_3O_4, GPTES-Fe_3O_4 and MNCPPA4-10% and MNCPPA4-20%.

Materials and Methods

Chemicals and reagents

All chemicals were purchased from Fluka and Merck Chemical Co. (Germany). 1,1-diphenyl-2-picrylhydrazyl (DPPH), 2-amino-4,6-dihydroxypyrimidine, (3-

glycidyloxypropyl) trimethoxysilane (GPTES), 9-ethyl-3-carbazolecarboxaldehyde, terphthalic acid, isophthalic acid, pyridine-2,6-dicarboxylic acid, 4,4'-sulfonyldibenzoic acid, adipic acid and sebacic acid were used as received. *N*-methyl-2-pyrrolidone (NMP), *N*,*N*-dimethylacetamide (DMAc), and pyridine (Py) were purified by distillation under reduced pressure over calcium hydride and stored over 4 Å molecular sieves. The ionic liquid, [1, 3-$(pr)_2$im]Br, was prepared according to the procedure reported in the previously paper.[6]

Synthesis

Synthesis of monomer (DATPhP), poly(pyrimidine-amide)s (PPAs), Fe_3O_4 nanoparticles and GPTES-Fe_3O_4 are reported in **ESI** in sections **S1**, **S2**, **S3**, and **S4,** respectively.

Preparation of GPTES-Fe_3O_4/PPA nanocomposites

A solution of 0.1 g PPA in 20 mL dry DMAc was prepared by stirring in a 150 W water ultrasonic bath for 30 min. Then a certain amount of modified GPTES-Fe_3O_4 nanoparticles (5, 10, 15 and 20 wt% based on weight of PPA) was added to the resulting solution and the mixture was ultra sonicated for 30 min at 70 °C. After irradiation, the mixture was continuously stirred at 70 °C for 5 h under N_2 atmosphere. Then solvent was removed, and the obtained nanocomposite was dried in a vacuum oven at 80 °C for 24 h. The schematic illustration of preparation of modified GPTES-Fe_3O_4 and nanocomposite is shown in **Scheme 1**.

Measurements

^{1}H NMR and ^{13}C NMR spectra were recorded on a 400 MHz and 100 MHz, respectively, Bruker Avance DRX instrument (Germany) using DMSO-d_6 as solvent and tetramethyl silane as an internal standard. FT-IR spectra were recorded using a Bruker

Tensor 27 spectrometer on KBr pellets over the range of 400-4000 cm^{-1}. Elemental analyses performed by a CHN-600 Leco elemental analyzer. Inherent viscosities (at a concentration of 0.5 g/dL) were measured with an Ubbelohde suspended-level viscometer at 25 °C using NMP as solvent. Solubility was determined using 0.05 g of a polymer in 0.5 mL of solvent. For the moisture absorption measurement, 200 mg polymer powder was dried at 120 ºC for 8 h and then placed in an open space with a relative humidity of 80% and weighed periodically over the course of 48 h. The GPC measurements were conducted at 30 ^{o}C with a Perkin-Elmer instrument equipped with a differential refractometer detector. The columns used were packed with a polystyrene/divinylbenzene copolymer (PL gel MIXED-B from Polymer Laboratories) with DMF as fluent at a flow rate of 1 mL/min. Calibration of the instrument was done with monodisperse polystyrene standards. Thermogravimetric analysis (TGA) was performed in temperature range of 30-650 °C with the DuPont Instruments (TGA 951) at 10 °C/min under N_2 (20 cm^3/min) and in air. Differential scanning calorimeter (DSC) was recorded on a Perkin Elmer pyres 6 DSC under N_2 (20 cm^3/min) at 10 °C/min. Glass-transition temperatures (T_g) values were read at the middle of the transition in heat capacity and were taken from the second heating scan after cooling from 350 °C at a cooling rate of 20 °C min^{-1}. UV-visible absorption and fluorescence emission spectra were recorded on a Cecil 5503 (Cecil Instruments, Cambridge, UK) and Perkin-Elmer LS-3B spectrophotometers (Norwalk, CT, USA) (slit width= 2 nm), respectively, using a dilute polymer solution (0.20 g/dL) in DMSO. To prepare crack-free and homogeneous thin films for the measurement of optical properties, solutions were made by dissolving about 0.5 g of polymer in 5 mL DMF to afford an approximate 10 wt% solution. The homogeneous solution was poured

into a 9 cm-diameter glass culture dish, heated under vacuum at 50 °C for 2 h, 100 °C for 5 h, and 150 °C for 3 h to evaporate the solvent slowly. Polymer films were self-stripped off from the glass surface by soaking in water. The polymer films were further dried in vacuum oven at 170 °C for 10 h. X-ray powder diffraction patterns were recorded by an X-ray diffractometer (GBC MMA instrument) with Be-filtered Cu K (1.5418 A°) operating at 35.4 kV and 28 mA. The 2θ scanning range was set between 4° and 50° at a scan rate of 0.05° pers. Atomic force microscopic (AFM) Easy Scan 2 Flex AFM (Swiss Co), was used to investigate the surface phase and topography of the nanocomposites. Branson S3200 (50 kHz, 150 W) ultrasonic bath was used for better dispersion of nanoparticles. Tensile properties, strips (width = 5 mm, length = 30 mm and thickness = 30-50 μm) were measured by using MTS Criterion™ Universal Test Systems with an extension rate of 5 mm min^{-1} and gauge length of 10 mm at 20 °C. At least six samples were tested for each polymer and the average values are reported. Antioxidant activity was measured using the DPPH assay. Briefly 1, 3, 5, 8 and 10 mg of PPA5 and MNCPPA5-5% nanocomposite samples were added to 3 mL of 100 μM solution in ethanol. The mixture was vortexed for 2 min to initiate the surface reaction between the sample and DPPH, which was followed by centrifugation at 5000 rpm for 2 min. Then, the absorbance of the supernatant was measured at 517 nm using a UV-vis spectrophotometer. It was made sure that all the measurements were taken at exactly 30 min after dissolving the sample in DPPH solution. The antimicrobial activities of the synthesized compounds were evaluated against *P. aeruginosa, S. aureus* (Gram negative bacteria), *K. pneumoniae* (gram negative bacteria), *A. oryzae*, and *A. niger* (fungi). An aliquot 0.1 mL of each bacterial strain was spread on nutrient agar, while 0.1 mL of the

fungal spore suspension was spread on potato dextrose agar (PDA). An agar-well diffusion test was performed in each case. In these tests, 6 mm wells were produced using a sterile cork borer, and each well was then inoculated with 100 μL of each key substance in DMF. Nutrient agar plates were incubated at 37 ºC for 24 h, while the PDA plates incubated at 25 ºC for 72 h. The zone of inhibition (in mm) was compared with the standard gentamycin and fluconazole for antibacterial and antifungal activities, respectively.

Conclusions

In this work, selective polyamidation of a multifunctional compound (DATPhP) in the mixture of IL/TPP led to preparation of poly(pyrimidine-amide)s (PPA)s. The PPAs with M_w in the range of 28375-49448 g/mol exhibited excellent solubility in common organic polar solvents and good thermal stability based on their T_g (174-257 °C) and $T_{10\%}$ values (420 - 458 ºC). The PPAs bearing different functional groups in their backbones were used for the preparation of reinforced magnetic nanocomposites with epoxide functionalized Fe_3O_4 nanoparticles. As compared with the PPAs, the tensile strength of nanocomposites improved significantly as a result of interfacial bonds between epoxide groups of GPTES-Fe_3O_4 and tertiary amines in the DATPhP unit of PPA chains. It has also been demonstrated that DATPhP, PPAs and the nanocomposite can act efficiently as antioxidant and antimicrobial materials.

Acknowledgements

The authors would like to thank the Mazandaran University of Medical Sciences, Faculty of Pharmacy (Iran) for use of its facilities to carry out antimicrobial tests.

References:

1 P. Wasserscheid and T. Welton, *Ionic liquids in synthesis*; Wiley-VCH Verlag GmbH & Co. KGaA, Weinheim, 2002; Ch. 7.

2 P. Kubisa, *Prog. Polym. Sci.,* 2009, **34**, 1333-1347.

3. P. Kubisa, *Prog. Polym. Sci.,* 2004, **29**, 3-12.

4 Y. S. Vygodskii, E. I. Lozinskaya and A. S. Shaplov, *Macromole. rapid. comm.,* 2002, **23**, 676-680.

5 E. I. Lozinskaya, A. S. Shaplov and Y. S. Vygodskii, *Eur. Polym. J.* 2004, **40**, 2065-2075.

6 M. Taghavi, M. Ghaemy, S. M. Amini Nasab and M. Hassanzadeh, *Polymer,* 2013, **54**, 3828-3840.

7 S. Mallakpour and M. Taghavi, *Polymer,* 2008, **49**, 3239-3249.

8 M. Ghaemy, M. Hassanzadeh, M. Taghavi and S. M. Amini Nasab, *J. Fluorine Chem.,* 2012, **142**, 29-40.

9 E. I. Lozinskaya, A. S. Shaplov, M. V. Kotseruba, L. I. Komarova, K. A. Lyssenko, M. Y. Antipin and Y. S. Vygodskii, *J. Polym. Sci., Part A: Polym. Chem.,* 2006, **44**, 380-394.

10 E. M. Dukuzeyezu, H. Lefebvre, M. Tessier and A. Fradet, *Polymer,* 2010, **51**, 1218-1221.

11 S. Zhang, V. Lemaire, A. Féret, H. Lefebvre, M. Tessier and A. Fradet, *Polym. Chem.,* 2013. **4**, 1538-1545

12 S. Zhang, H. Lefebvre, M. Tessier and A. Fradet, *Green Chem.,* 2011, **13**, 2786-2793.

13 R. Marcilla, M. de Geus, D. Mecerreyes, C. J. Duxbury, C. E. Koning and A. Heise, *Eur. Polym. J.,* 2006, **42**, 1215-1221.

14 M. Yoshizawa-Fujita, C. Saito, Y. Takeoka and M. Rikukawa, *Polym. Adv. Technol.,* 2008, **19**, 1396-1400.

15 S. S. Panda and P. V. Chowdary, *Indian J. Pharm. Sci*., 2008, 70, 208-15.

16 S. Ostrowski, *Jordan J. Chem.,*. 2013, **3**, 349-355.

17 A. Moskvin, N. Reznikova, M. Meshcheryakov and B. Ivin, *Russ. J. Gen. Chem.,* 2001, **71**, 1096-1098.

18 A. H. Lu, E. L. Salabas and F. Schuth, *Angew. Chem. Int. Ed*., 2007, **46**, 1222-1244.

19 A. K. Gupta and M. Gupta, *Biomaterials,* 2005, **26**, 3995-4021.

20 S. Mornet, S. Vasseur, F. Grasset, P. Veverka, G. Goglio, A. Demourgues, J. Portier, E. Pollert and E. Duguet, *Prog. Solid State Chem*., 2006, **34**, 237-247.

21 E. Amstad, M. Textor and E. Reimhult, *Nanoscale,* 2011, **3**, 2819-2843.

22 O. Veiseh, J. W. Gunn and M. Zhang, *Adv. Drug Deliv. Rev*., 2010, **62**, 284-304.

23 X. L. Liu, E. S. G. Choo, A. S. Ahmed, L.Y. Zhao, Y. Yang, R. V. Ramanujan, J. M. Xue, D. D. Fan, H. M. Fan and J. Ding, *J. Mater. Chem.,* 2014, **2**, 120-128.

24 S. Paul, J. P. Saikia, S. K. Samdarshi and B. K. Konwar, *J. Magn. Magn. Mater*., 2009, **321**, 3621-3623.

25 A. Masoumi, M. Ghaemy and A. Nik Bakht, *Ind. Eng. Chem. Res*., 2014, **53**, 8188−8197.

26 S. Wang, Y. Zhou, W. Guan and B. Ding, *J. Nanopart. Res.,* 2008, **11**, 909-916.

27 N. Yamazaki, M. Matsumoto and F. Higashi, *J. Polym. Sci., Part A: Polym. Chem.,* 1975, **13**, 1373-1380.

28 F. Ricciardi, W. A. Romanchick, M. M. Jouille, *J. Polym. Sci. Polym. Chem. Ed.*, 1983, **21**, 1475-1490.

29 M. Ghaemy, S. Sadjady, *J. Appl. Polym. Sci.,* 2006, **100**, 2634-2641.

30 B. Y. Ryu, T. Emrick, *Macromolecules*, 2011, **44**, 5693-5700.

30 G. S. Liou and C. W. Chang, *Macromolecules,* 2008, **41**, 1667-1674.

31 K. Bhattacharya, B. Gogoi, A. K. Buragohain and P. Deb, *Mater. Sci. Eng. C.,* 2014, **42**, 595-600.

32 S. A. Raghunath, Y. Manjunatha and K. Rayappa, *Med. Chem. Res.,* 2011, **21**, 3809-3817.

33 D. W. Van Krevelen and K. T. Nijenhuis, *Properties of polymers*; Elsevier Scientific Publishing: Amsterdam, 2008.

34 M. Li, L. Q. Xu, L. Wang, Y. P. Wu and E. T. Kang, *Polym. Chem.,* 2011, **2**, 1312-1321.

Captions

Scheme 1. Illustration of synthesis of target DATPhP, PPAs and chemically bonded nanocomposites.

Fig. 1. FT-IR spectra of mNP, DATPhP, PPA and nanocomposite.

Fig. 2. DSC (A) and TGA (B) curves of GPTES-Fe_3O_4/PPA, PPAs and nanocomposite under N_2 at 10 ^oC/min.

Fig. 3. FESEM image of Fe_3O_4 (A), GPTES-Fe_3O_4 (B), MNCPPA4-20% (C) and TEM image of MNCPPA4-20% (D).

Fig. 4. UV-vis and fluorescence spectra of PPAs and nanocomposites.

Fig. 5. Antioxidant properties of DATPhP, PPA1, PPA4 and MNCPPA4-5%.

Fig. 6. DMTA curves of tan δ and storage modulus of PPA1, PPA5 and NCPA5-10%.

Fig. 7. VSM images of Fe_3O_4, GPTES-Fe_3O_4 and MNCPPA4-10% and MNCPPA4-20%.

Captions in ESI

Fig. 1S. ^1H NMR (A) and ^{13}C NMR (B) spectrum of DATPhP in DMSO-d_6.

Fig. 2S. ^1H NMR spectrum of PPA4 (A) and PPA5 (B) in DMSO-d_6.

Fig. 3S. X-ray diffraction patterns of Fe_3O_4, mNS, PPA6 and MNCPA6-20%.

Fig. 4S. AFM images of GPTES-Fe_3O_4, MNCPPA4-20%.

Scheme 1S. Mechanism of antioxidant activity.

For "Table of Contents" use only

Preparation and properties of magnetic Fe_3O_4/poly(pyrimidine-amide) nanocomposites: selective polyamidation of a bis(amino-pyrimidine-diol) compound in an ionic liquid

Mehdi Taghavi, Raouf Alizadeh and Mousa Ghaemy*

Polymer Chemistry Research Laboratory, Faculty of Chemistry, University of Mazandaran, Babolsar, 47416-95447, Iran

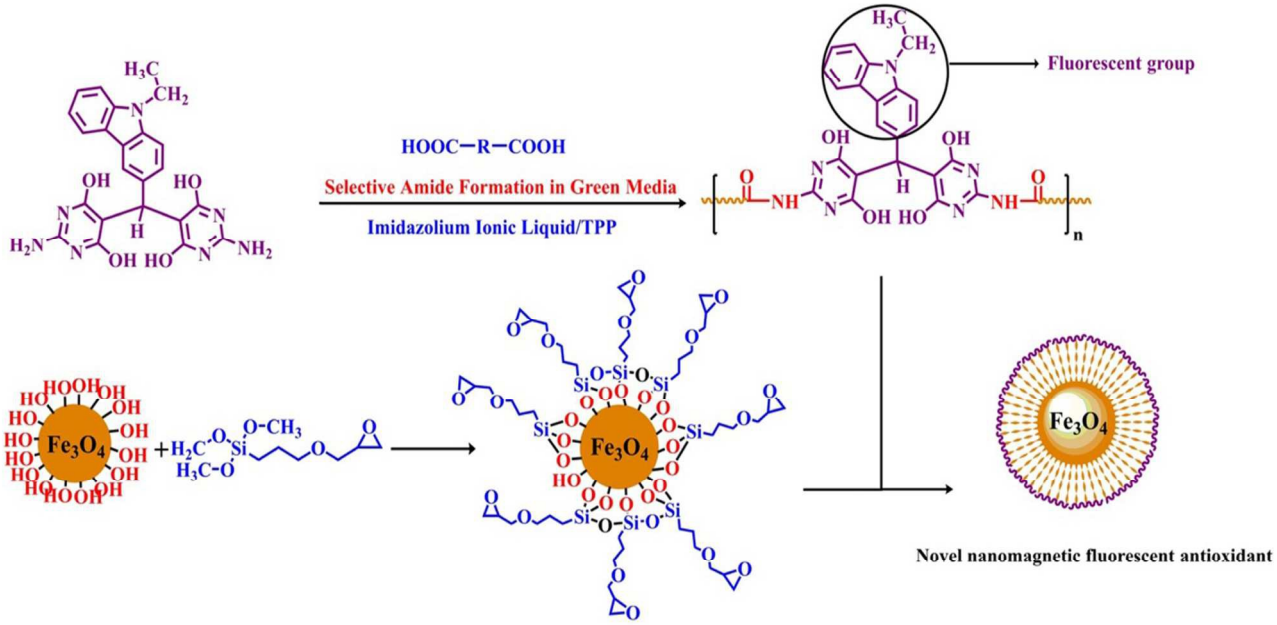

* Corresponding author. Tel.: +98-112-5342353; FAX: +98-112-5342350.
E-mail address: ghaemy@umz.ac.ir (Mousa Ghaemy).